PHYSICAL REVIEW B **83**, 174512 (2011)

Polymorphism in $BaPb_{1-x}Bi_xO_3$ at the superconducting composition

E. Climent-Pascual,[1] N. Ni,[1] S. Jia,[1] Q. Huang,[2] and R. J. Cava[1]

[1]*Department of Chemistry, Princeton University, Princeton, New Jersey 08544, USA*

[2]*NIST Center for Neutron Research, National Institute of Standards and Technology, Gaithersburg, Maryland, 20899, USA*

(Received 21 February 2011; revised manuscript received 30 March 2011; published 16 May 2011)

Using a combination of high-resolution and high-sensitivity neutron and x-ray diffraction measurements, it is shown that $BaPb_{1-x}Bi_xO_3$ is dimorphic for the critical superconducting composition regime of x between 0.2 and 0.3. The system is not chemically phase separated; the simultaneous existence of tetragonal and orthorhombic polymorphs of the same composition is demonstrated. The polymorphs differ fundamentally in the distortion and tilting of the octahedra, such that they cannot be obtained from each other via a second-order phase transition. It is established that the tetragonal symmetry polymorph is the superconducting phase.

DOI: 10.1103/PhysRevB.83.174512 PACS number(s): 74.70.−b, 61.05.cp, 61.05.F−, 61.50.Ks

I. INTRODUCTION

Over the past 30 years, the prototype charge-disproportionated perovskite system $BaPb_{1-x}Bi_xO_3$ (BPBO) has attracted interest due to its exhibition of a metal-semiconductor (M-S) transition ($x \approx 0.35$) (Ref. 1) and three-dimensional superconductivity ($0 < x \leqslant 0.30$) with a relatively high superconducting transition temperature ($T_C \simeq 13$ K for x near 0.25),[2] in spite of its low carrier concentration and remarkably low density of states at the Fermi level.[3–5] For $x < 0.35$ (in the metallic state), the hypothetically present Bi(IV) is disproportionated into Bi(III) and Bi(V), giving rise to a strong real space electron-pairing interaction by trapping of two electrons on one site through local lattice relaxations. This results in the local existence of three different octahedral complexes, $Pb(IV)O_6$, $Bi(V)O_6$, and $Bi(III)O_6$, and the free motion of carrier pairs by dynamic exchange through the $Pb(IV)O_6$–$Bi(V)O_6$ system. Thus, in a local picture, the correlation between the movement of carrier pairs and oxygen octahedra "breathing" vibrations may be invoked as the origin of the superconductivity in BPBO for $0 < x \leqslant 0.30$. At higher values of x, the number of large $Bi(III)O_6$ complexes and the pair localization energy rise, and the system therefore becomes a semiconductor due to progressive localization of the carriers [see, for example, Refs. 6–11].

Although it is not the usual "k-space" picture of superconductivity, the local real space effects described above have been often invoked to describe the structure-property relationships in the BPBO system. Detailed correlations between the average crystal symmetry and the electrical properties, usually the entry point for the in-depth k-space analysis of electronic materials, have not, however, been clearly established for BPBO. Although electronic structure calculations based on ideal cubic perovskite symmetry and tetragonal symmetry have been performed, they did not find a profound impact of symmetry on the density of states at the Fermi energy.[12] It cannot be the case that structural symmetry is irrelevant for bismuthate superconductors, however, because the dramatic difference in T_C between cubic $Ba_{0.6}K_{0.4}BiO_3$ [30 K (Refs. 13 and 14)] and tetragonal $Sr_{0.4}K_{0.6}BiO_3$ [12 K (Ref. 15)], which differs significantly only in symmetry, indicates otherwise.

The problem with establishing clear structure-property correlations in BPBO, the first bismuthate superconductor, is that the structural distortions from ideal perovskite cubic symmetry are subtle and difficult to ascertain in this system. To establish clearly the symmetry and average structure for the BPBO superconductor through the use of optimized diffraction methods is the aim of our study. The phase diagram of the distorted perovskite BPBO system has been studied since 1975,[2] and though it can basically be described as a perovskite supercell with $a \approx b \approx \sqrt{2}a_{pc}$ and $c \approx 2a_{pc}$, where a_{pc} is the pseudocubic perovskite lattice parameter, the composition dependence of the crystal structure in this family remains highly controversial. It has been reported that $BaPb_{1-x}Bi_xO_3$ undergoes a series of not clearly established structural phase transitions between tetragonal, orthorhombic, and monoclinic phases at room temperature (RT) as a function of the bismuth doping. Cox and Sleight[16] reported that $BaPb_{1-x}Bi_xO_3$ is orthorhombic for $0 < x < 0.05$, tetragonal for $0.05 < x < 0.35$, orthorhombic again for $0.35 < x < 0.9$ and finally, monoclinic for $x \geqslant 0.9$. These authors reexamined the structure for $x \approx 0.275$ and 0.3 some years later and reported that they were unable to obtain single-phase samples around the critical composition range for superconductivity ($x \approx 0.25$)[17]; they always observed a mixture of tetragonal and orthorhombic phases. Khan *et al.*[1] and Oda *et al.*[18] independently concluded that the orthorhombic structure extends over the whole range of compositions $0 < x < 0.9$. Later, Oda *et al.*[19] and Asano *et al.*[20] proposed that the tetragonal structure in the $0.05 < x < 0.35$ composition range can transform to an orthorhombic one, depending on the sample preparation. They also claimed that the T_C values of the tetragonal and orthorhombic phases are different. Moreover, they reported that both phases can transform to monoclinic symmetry at low temperatures. Ihringer *et al.*[21] and Ritter *et al.*[22] concluded that the structure is monoclinic for $0 < x < 0.25$. Marx *et al.*[23] proposed a RT structural phase diagram where BPBO is monoclinic for $0 < x < 0.2$, diphasic (tetragonal plus orthorhombic) for the critical composition range of the superconductivity $0.2 < x < 0.35$, orthorhombic for $0.35 < x < 0.8$, and monoclinic again for $x > 0.8$. They also concluded that the structure is single-phase tetragonal above 450 K but that the tetragonal-to-orthorhombic phase transition never proceeds to completion, and for this reason BPBO near the superconducting compositions, $0.2 < x < 0.35$, is always a diphasic mixture. The most striking feature of this latter study is that the authors concluded that only the tetragonal phase is superconducting, which disagrees

with the study carried out by Oda *et al.*[18] More recently, Medicherla *et al.*,[24] Moussa *et al.*,[25] and Fu *et al.*[26] have claimed that the end member $BaPbO_3$ ($x = 0$) is orthorhombic at RT rather than monoclinic. Moreover, Moretzki *et al.*[27] reported that the RT structure is tetragonal in BPBO for $x \approx 0.1$.

The confusion engendered by these conflicting reports provides a discouraging starting point for the detailed analysis of structure-property correlations in the BPBO system. Considering the information available, it is important to note that the controversy is most pronounced around the compositions that exhibit optimal superconductivity, $0.2 < x < 0.30$, where many researchers argue that at RT a mixture of tetragonal and orthorhombic phases seems to always be present. The crystal structures of the tetragonal and orthorhombic phases near the superconducting composition have been described by the space groups $I4/mcm$ (no. 140) and *Ibmm* (no. 74), respectively,[16–19,23] but the understanding of the possible relationships between them and a detailed analysis of the compositions of these phases remain lacking. Given the strong competition between structural phases and electronic states that the BPBO system represents, arguably one of the strongest cases of this phenomenon known is that it is important to establish whether or not there is chemical phase separation, structural instability, or electronic phase separation in the critical composition region for superconductivity.

Here we demonstrate, using a combination of high-resolution and high-sensitivity neutron and x-ray diffraction measurements, that the BPBO system for the critical superconducting composition regime of x between 0.2 and 0.3 is a dimorphic rather than a phase-separated system, showing the coexistence of tetragonal and orthorhombic polymorphs of the same composition but not chemical phase separation. This confirms and augments some of the previous studies. We show that the orthorhombic and tetragonal polymorphs differ fundamentally in the distortion and tilting of the octahedra, such that they cannot be obtained from each other via a second-order phase transition, therefore explaining the dimorphic nature of the system at room temperature. Finally, by investigating different samples in the critical composition regime, we establish that the quality of the superconductivity is correlated with the tetragonal polymorph content, indicating that the tetragonal symmetry polymorph is the superconducting phase.

II. EXPERIMENTAL

Fifteen-gram powder samples of $BaPb_{1-x}Bi_xO_3$ compounds for $0 \leqslant x \leqslant 0.6$ ($x = 0$, 0.15, 0.2, 0.225, 0.25, 0.275, 0.3, 0.35, and 0.6) were prepared by heating stoichiometric amounts of $Ba(NO_3)_2$ (99.999%; Alfa Aesar), $Pb(NO_3)_2$ (99.999%; Alfa Aesar), and Bi_2O_3 (99.8%; Aldrich) in oxygen at a flow rate of about 1 $cm^3\ s^{-1}$.[28] The powders were mixed and ground together in an agate mortar and, after an initial heat treatment at 873 K for 24 h, the powder was reground, pressed into pellets, and reheated at 1123 K for 96 h (with regrinds every 24 h) followed by slowly cooling to RT.

The purity, symmetry, and cell parameters of the samples obtained were evaluated by means of x-ray powder diffraction data collected at RT on a Bruker D8 FOCUS diffractometer (Cu Kα) over a 2θ range between 5 and 110° with a step size of 0.014°. The superconductivity was studied by means of ac and dc magnetization measurements using a quantum design (QD) physical properties measurement system (PPMS) and a QD magnetic properties measurement system (MPMS) superconducting quantum interference device (SQUID) magnetometer, respectively. The magnetic measurements were carried out in low magnetic fields (H), 5 and 2 Oe for ac and dc measurements, respectively. The measurements strongly depend on the shape and size of the sample; thus about 53 mg of BPBO for x between 0.15 and 0.35 were pressed into slab-pellets (0.5 cm diameter and 0.1 cm thick), sintered in oxygen flow (1 $cm^3\ s^{-1}$) at 1000 K for 6 h, and oriented with the diameter parallel to the applied magnetic field (demagnetization factor $N \approx 0$). DC measurements were performed in the field-cooled (FC) mode. The remnant fields were estimated using a palladium reference sample. The superconducting volumes were estimated from the dc-FC susceptibility measurements as a fraction of the full diamagnetism $4\pi\chi_v = -1$. The volume normalization was carried out using the calculated densities for each sample. Neutron powder diffraction (NPD) experiments were performed on the high-resolution powder diffractometer BT1 ($\lambda \simeq 2.0783$ and 1.1968 Å) at the Center for Neutron Research of the National Institute of Standard and Technology (NIST) at Gaithersburg, MD, USA. Samples for $x = 0.20$, 0.25, and 0.3 were loaded into vanadium containers and data were collected at RT over a 2θ range between 3 and 166° with a step size of 0.05°. Lattice parameters, atomic positions, occupancy factors, and atomic displacement factors were refined by the Rietveld method using the FULLPROF program integrated in the WINPLOTR software.[29] Diffraction maxima were fit with the Thompson-Cox- Hastings pseudo-Voigt function starting from the instrumental resolution values for the profile parameters U, V, W, and Y. These starting profile parameters were obtained by fitting data obtained for sintered samples of alumina with smaller broadening effects and supplied by NIST. The background was characterized by use of a 12-coefficient polynomial function.

III. RESULTS AND DISCUSSION

The x-ray powder diffraction (XRPD) patterns for all BPBO samples indicate that pure perovskite-like materials were obtained. The XRPD patterns for $x = 0$, 0.35, and 0.60 were indexed to an *Ibmm* orthorhombic supercell ($a \approx b \approx \sqrt{2}a_p$ and $c \approx 2a_p$), apparent in the splitting of the pseudocubic 200 and 222 reflections into the orthorhombic 220 and 004, and 404 and 044 reflections, respectively, as shown in Fig. 1. The supercell arises from the tilting of the $Pb[Bi]O_6$ octahedra, $a^-a^-c^0$ in Glazer's notation,[30] a set of rotations that is out-of-phase (–) around the $[110]_{pc}$ pseudocubic axis. For x between 0.15 and 0.30 the XRPD patterns were initially indexed to an $I4/mcm$ ($a^-a^-c^0$) tetragonal supercell ($a = b \approx \sqrt{2}a_p$ and $c \approx 2a_p$), where the distortion consists only of rotations around the $[001]_{pc}$ axis. In this case the pseudocubic 200 reflection is split into the tetragonal reflections 004 and 220, but the 222 reflection remains unsplit. However, a close examination of the XRPD patterns in this composition range revealed that the reflections corresponding to the *Ibmm* orthorhombic phase are also present (Fig. 1). These data

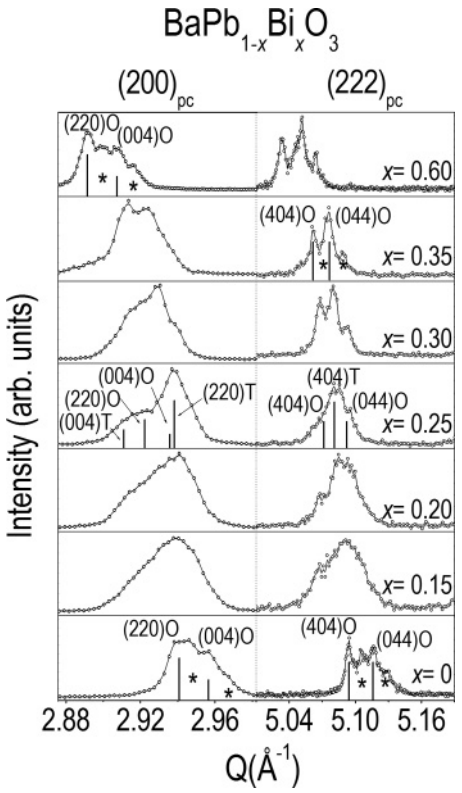

FIG. 1. Portions of the XRPD patterns of BPBO for x between 0 and 0.35, and 0.6 at 300 K. Open circles represent the experimental data and the vertical marks indicate the allowed Bragg reflections (Cu Kα_1) in *Ibmm* (O) and *I*4/*mcm* (T). These reflections have been indexed on basis of the splitting of the pseudocubic reflections 200 and 222. The asterisks indicate the Cu Kα_2 radiation contribution to the patterns.

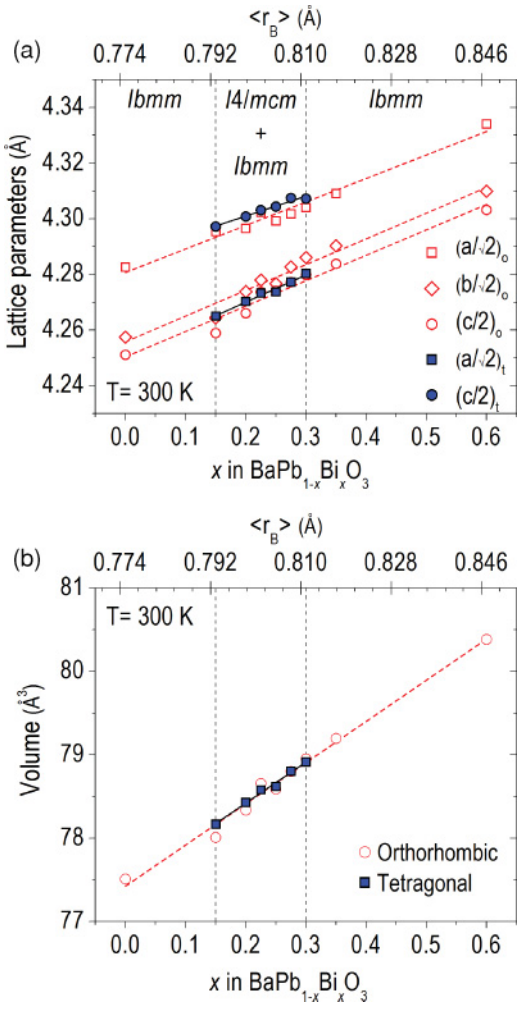

FIG. 2. (Color online) Variation of the reduced lattice parameters (a) and volume (b) with composition and the average radius at B-type site $\langle r_B \rangle$ for the orthorhombic and tetragonal polymorphs of BPBO for $0 \leqslant x \leqslant 0.6$. These were estimated from XRPD data (Cu Kα); the standard deviations are smaller than the size of the symbols. The vertical dashed lines indicate the two-phase region. The dashed lines are guides to the eye.

then clearly confirm the previously reported[16,23] coexistence of the tetragonal and orthorhombic phases for $0.15 < x \leqslant 0.30$. The composition dependence of the reduced lattice parameters and cell volume are depicted in Fig. 2, refined by the Rietveld profile fit refinement option using XRPD data and taking into account the two-phase region limits. A most remarkable feature of the data in Fig. 1 is that both the lattice parameters and cell volume increase continuously with increasing effective size of the cation at the B-type site (i.e., the bismuth content). This shows that there is no chemical phase separation in this composition region; in that event the lattice parameters and cell volume would be constant across this region with only their relative proportions changing. This result is consistent again with previous studies and supports the two-polymorph (tetragonal plus orthorhombic) scenario rather than one of phase separation over a chemical two-phase region. The second notable feature in the composition variation of the reduced lattice parameters is the change of the reduced lattice parameter c/a ratio from $(c/a)_o < 1$ (orthorhombic) to $(c/a)_t > 1$ (tetragonal) over the two-polymorph range. Since the differences in these structures involve an abrupt change of the tilting of the octahedra from a diad axis ($a^-a^-c^0$) to a tetrad axis ($a^-a^-c^0$), the transformation from *Ibmm* to *I*4/*mcm* is first-order displacive;[31–35] that is, the octahedral rotation axis instantaneously moves 90° at the phase transition from the $[110]_{pc}$ pseudocubic axis in *Ibmm* to $[001]_{pc}$ in *I*4/*mcm*, shown in Fig. 3. In this sense, a difference between the reduced cell volumes corresponding to the orthorhombic and tetragonal phases is observed for $0.15 < x \leqslant 0.25$, which is indicative again of a first-order transition. Taking into account this first-order movement of the rotation axis and considering that the projection of the octahedra onto the (001) plane in the orthorhombic phase coincides with the (110) plane in the tetragonal phase (Fig. 3), the possible existence of a two-polymorph region is not so surprising for the BPBO system and has been observed in other systems such as $SrRuO_3$, $Sr_{0.5}Ba_{0.5}HfO_3$, $Sr_{1-x}Ca_xTiO_3$ and $Sr_{1-x}Ba_xZrO_3$.[33,36–39] The two-polymorph region suggests a relatively small difference in energy between the orthorhombic and tetragonal polymorphs of the BPBO perovskite right in the superconducting composition region, indicating a competition between the tilt systems around the diad axis and the tetrad axis when the orthorhombic polymorph becomes pseudotetragonal

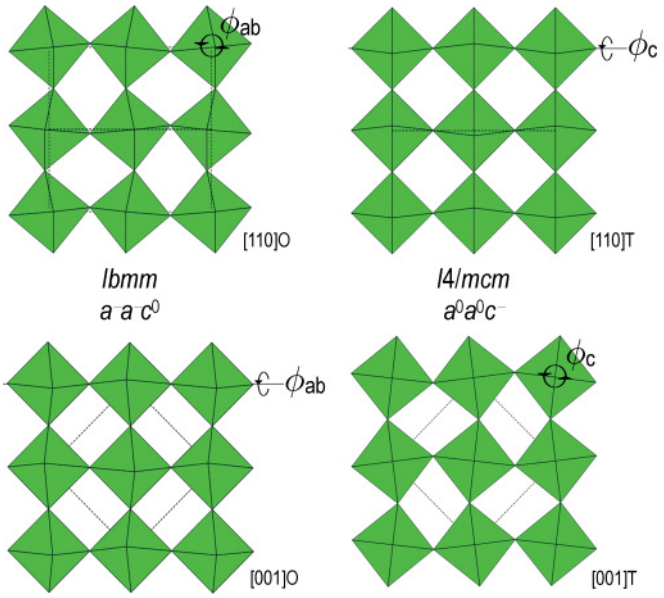

FIG. 3. (Color online) Projections of the perovskite structure for the orthorhombic *Ibmm* and tetragonal $I4/mcm$ symmetries along [110] and [001] (O = orthorhombic and T = tetragonal). The octahedra represent Pb[Bi]O_6. $a^-a^-c^0$ and $a^0a^0c^-$ denote Glazer 's notation for *Ibmm* and $I4/mcm$. The arrows indicate the tilt angles (ϕ) for both symmetries.

($x \approx 0.20$; $\langle r_B \rangle \approx 0.799$ Å, where $\langle r_B \rangle$ is the effective cation size at the B-type site using $r_{Pb(IV)} = 0.775$ Å, $r_{Bi(III)} = 1.03$ Å, and $r_{Bi(V)} = 0.76$ Å for CN = 6).[40] Hence, the phase transition is apparently driven by $\langle r_B \rangle$. It is important to note that BPBO undergoes the *Ibmm*–$I4/mcm$ transition due to rotational instabilities rather than ferroelectric, Jahn-Teller, and other electronic distortions.

In order to complete the study of the cation-size controlled phase transitions in $BaPb_{1-x}Bi_xO_3$, both high ($\lambda \simeq 2.0783$ Å) and medium ($\lambda \simeq 1.1968$ Å) resolution NPD data were recorded for $x = 0.20$, 0.25, and 0.30 at RT. Both patterns for each composition were analyzed by a combined multipattern Rietveld refinement. This method allows for the simultaneous determination of both the symmetry and the compositions of the phases. The Rietveld fits for both NPD data sets for $BaPb_{1-x}Bi_xO_3$ ($x = 0.20$, 0.25, and 0.30) at RT are shown in Fig. 4. These refinements were based on the orthorhombic and tetragonal structural models previously reported by Marx *et al.*[23] for BPBO. In order to refine the compositions of both phases, the occupancy factors of the cations at the perovskite B site were weakly constrained by setting the lead content as $n_{Pb} = 1 - n_{Bi}$ (i.e., not allowing for B-site vacancies). The difference between the orthorhombic *Ibmm* and tetragonal $I4/mcm$ symmetries was analyzed in terms of the angle of rotation and distortion of the octahedra of this perovskite material. Though it would be possible to estimate the magnitudes of the tilts for rigid octahedra using the lattice parameters alone, previously reported results show clearly that the octahedra are not required to be regular. The tilt angles are therefore better estimated from the atomic positions of the oxygen atoms. In both symmetries the oxygen atoms are located on two independent sets of Wyckoff sites, which describe two apical O(1) and four basal plane O(2) atoms of

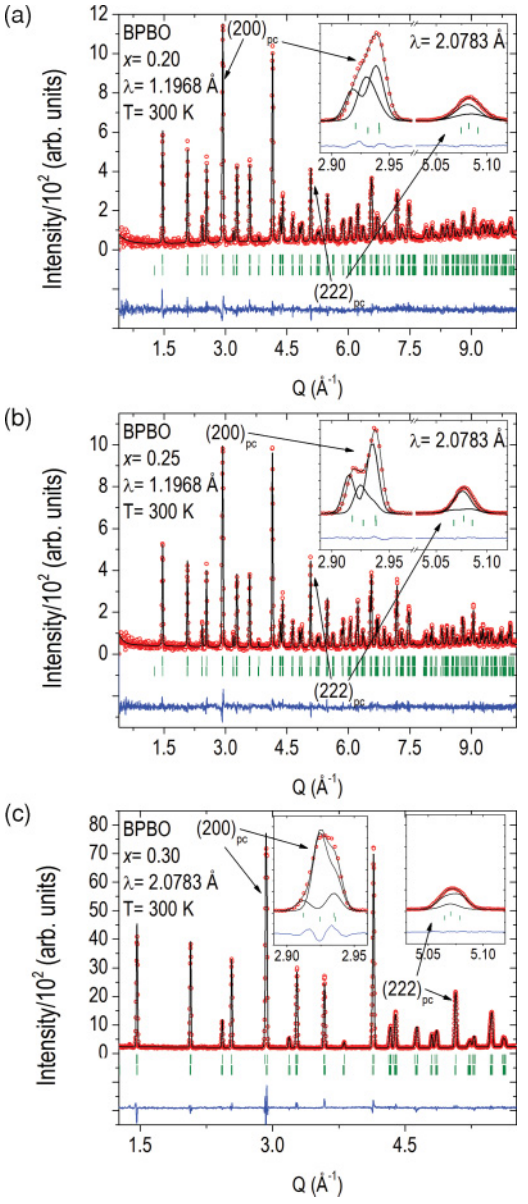

FIG. 4. (Color online) Observed (open circles), calculated (solid line) and difference (lower solid line) NPD ($\lambda \simeq 1.1968$ Å) profiles of BPBO for $x = 0.2$ (a), 0.25 (b), and 0.3 (c) at 300 K. Tick marks indicate the position of allowed reflections in $I4/mcm$ (upper) and *Ibmm* (lower). The insets show portions of the observed, calculated, and difference NPD ($\lambda \simeq 2.0783$ Å) profiles for the pseudocubic reflections 200 ($\rightarrow$ 004T+220O+004O+220T; T = tetragonal; O = orthorhombic) and 222 ($\rightarrow$ 404O+404T+044O). Dashed lines denote the contribution to the calculated profile of both symmetries.

the Pb[Bi]O_6 octahedra. Thus, in the orthorhombic symmetry structure, O(1) occupies the 4*e* site at (x, 0, 1/2) and O(2) occupies the 8*g* site at (1/4, 1/4, z) with two equal angles of rotation, ($\phi\phi$0 in Aleksandrov's notation)[41] of the octahedra around the axis parallel to a diagonal $\langle 110 \rangle_{pc}$ of the octahedral basal plane (Fig. 2). In the tetragonal symmetry structure, O(1) occupies the 4*a* site at (0, 0, 1/4) and O(2) occupies the 8*h* site at (x, x + 1/2, 0), with the only angle of rotation (00ϕ) of the octahedra about the axis parallel to $\langle 110 \rangle_{pc}$ (Fig. 2). Therefore the out-of-phase tilting of the octahedra

TABLE I. Refined lattice parameters, atomic positions, and atomic displacement parameters ($\times 10^2$ Å^2) of $BaPb_{1-x}Bi_xO_3$ ($x = 0.2$, 0.25, and 0.30) in tetragonal $I4/mcm$ and orthorhombic $Ibmm$ at 300 K. Agreement factors (R_{Bragg}, R_P, R_{wp}, and χ^2), strain of the orthorhombic cell (δ), and out-of-phase tilt angles ($\phi^-_{O(2)}$) are also given. In brackets are located the agreement factors corresponding to the multipattern Rietveld analysis of the NPD data using $\lambda = 1.1968$ Å, and without brackets those factors corresponding to the analysis using $\lambda = 2.0783$ Å.

Composition		$x = 0.20$		$x = 0.25$		$x = 0.30$	
Symmetry		*Ibmm*	*I*4/*mcm*	*Ibmm*	*I*4/*mcm*	*Ibmm*	*I*4/*mcm*
Fract. (wt%)		40(2)	60(2)	27(2)	73(2)	79(6)	21(7)
a (Å)		6.0858(3)	6.04273(14)	6.0855(2)	6.04752(8)	6.08974(8)	6.05557(19)
b (Å)		6.0418(4)		6.0545(2)		6.06488(8)	
c (Å)		8.5448(6)	8.6021(3)	8.5518(5)	8.61275(15)	8.56067(14)	8.63106(14)
V (Å^3)		314.18(3)	314.102(13)	315.09(2)	314.990(8)	316.176(8)	316.500(15)
δ (%)		0.73		0.51		0.40	
Ba	x/a	0.4988(19)		0.496(2)		0.4999(8)	
	U_{iso}	0.6(6)	0.9(3)	1.3(9)	0.7(2)	1.06(12)	0.3(4)
Pb[Bi]	n_{Pb}	0.80(3)	0.80(7)	0.72(3)	0.72(6)	0.70(4)	0.70(9)
	U_{iso}	1.1(3)	0.42(3)	0.8(6)	0.30(14)	0.69(4)	0.69(4)
O(1)	x/a	0.0493(17)		0.0496(17)		0.0436(6)	
	U_{iso}	1.3(5)	1.63(11)	1.6(8)	1.8(2)	1.44(7)	3.1(3)
O(2)	x/a		0.2796(6)		0.2801(4)		0.2866(14)
	z/c	0.9728(12)		0.9741(12)		0.9777(4)	
	U_{iso}	2.9(5)	1.43(17)	2.2(7)	1.44(17)	1.65(7)	2.1(3)
$\phi^-_{O(2)}$(deg.)		8.74	6.75	8.33	6.86	7.19	8.33
R_{Bragg} (%)		2.02[5.75]	1.56[6.40]	3.08[6.71]	2.43[6.38]	3.87	4.11
R_P (%)		5.17[8.34]		4.82[9.56]		5.14	
R_{wp} (%)		6.75[9.81]		6.50[11.8]		6.35	
χ^2		1.17[1.01]		1.06[1.03]		1.67	

$\tan\phi^-_{O(2)}$ (*Ibmm*) $= 4\sqrt{2}\omega$; $\tan\phi^-_{O(2)}$ (*I*4/*mcm*) $= 4\upsilon$; $\delta = 2(a–b)/(a+b)$

can be obtained from the O(2) atomic positions. For the orthorhombic *Ibmm* structure, the tilt about the diad axis is given by $\tan(\phi^-_{O(2)}) = 4\sqrt{2}\omega$, where $\omega = -z_{O(2)}$ (Ref. 42); while for the tetragonal *I*4/*mcm* structure the tilt angle about the tetrad axis can be estimated by $\tan(\phi^-_{O(2)}) = 4\upsilon$, where $\upsilon = x_{O(2)} - 1/4$ (Ref. 42). The distortion of the octahedra can be obtained by $\Delta_d = (1/6)\sum_{n=1,6}[(d_n - \langle d\rangle)/\langle d\rangle]^2$, where d_c, d_{ab}, and $\langle d\rangle$ are the axial, in-plane, and average Pb[Bi]–O bond distances in the octahedra. The final structural parameters along with the agreement factors are listed in Table I and a selected list of bond distances and angles is shown in Table II. The tilt and the distortion of the octahedra as well as the strain of the orthorhombic cell, $\delta = 2(a–b)/(a+b)$, are also included in those tables.

The n_{Pb} refined occupancy factor for the lead cation at the *B*-type site shows that the composition of both phases for each sample is close to the nominal one, within the standard deviations (Table I). This fact along with the gradual increase

TABLE II. Selected bond distances and angles estimated for $BaPb_{1-x}Bi_xO_3$ ($x = 0.2$, 0.25, and 0.30) from the Rietveld analysis of the NPD data at 300 K. d_c and d_{ab} denote the Pb[Bi]–O bond lengths along the c axis and within the ab plane. Θ_c and Θ_{ab} denote the Pb[Bi]–O–Pb[Bi] bond angles along the c axis and within the ab plane. The octahedral distortions ($\Delta_d \times 10^3$) are also included.

Composition	$x = 0.20$		$x = 0.25$		$x = 0.30$	
Symmetry	*Ibmm*	*I*4/*mcm*	*Ibmm*	*I*4/*mcm*	*Ibmm*	*I*4/*mcm*
d_c (Å)	2.1572(14)	2.151(6)	2.1592(15)	2.1532(10)	2.1566(10)	2.1402(10)
d_{ab} (Å)	2.1565(11)	2.151(4)	2.1575(11)	2.154(2)	2.1571(10)	2.164(8)
$\langle d\rangle$ (Å)	2.157	2.151	2.158	2.154	2.157	2.156
Δ_d (%)	0.04		0.14	0.05	0.01	2.71
Θ_c (deg.)	164.010(5)	180	163.93(4)	180	165.86(10)	180
Θ_{ab} (deg.)	166.63(10)	166.49(19)	168.22(10)	166.27(13)	169.84(10)	163.3(4)

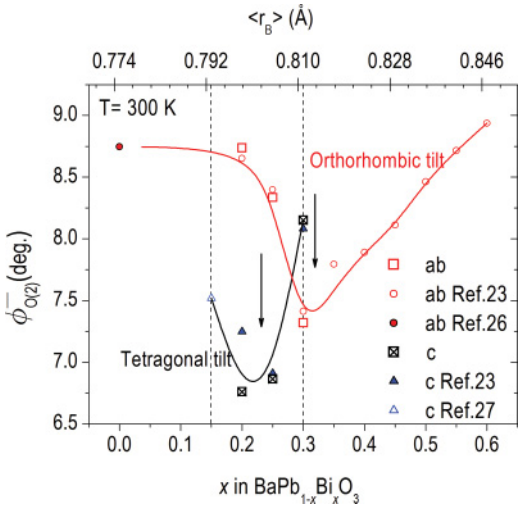

FIG. 5. (Color online) Variation of the tilt angle ($\phi^{-}_{O(2)}$) with composition and average radius at B-type site $\langle r_B \rangle$ for the orthorhombic and tetragonal polymorphs of BPBO for $0 \leqslant x \leqslant 0.6$. The composition for the highest T_C ($x \approx 0.25$) and the metal-to-semiconductor (M-S) transition ($x \approx 0.35$) are indicated by arrows. Data calculated from the results published by Marx *et al.*,[23] Fu *et al.*,[26] and Moretzki *et al.*[27] have been included. The vertical dashed lines indicate the two-phase region. The solid lines are guides to the eye.

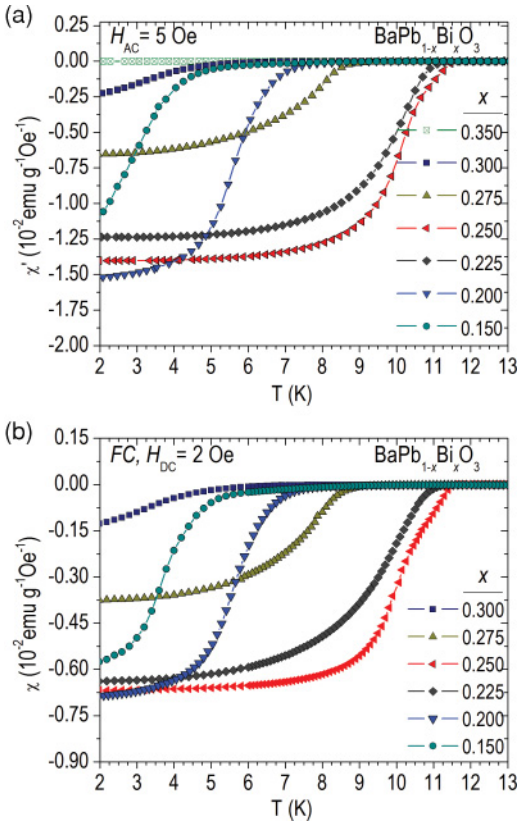

FIG. 6. (Color online) Temperature evolution of the ac magnetic susceptibility at $f \backsimeq 10$ kHz and $H_{ac} \backsimeq 5$ Oe (a) and the field-cooled dc magnetic susceptibility at $H_{\rm dc} = 2$ Oe (b) for BPBO, for $0.15 \leqslant x \leqslant 0.35$.

in the cell volume V confirms again the coexistence of the orthorhombic and tetragonal polymorphs for the $0 < x \leqslant 0.3$ composition range instead of chemical phase separation (Table I). The tetragonal polymorph appears as the main phase, ~70%, for $x \approx 0.20$ and 0.25, whereas its fraction drops to ~20% for $x \approx 0.3$. In other words, for $0.20 \leqslant x \leqslant 0.25$, the optimal superconducting composition regime, a competition between the orthorhombic ($\phi\phi 0$) and tetragonal (00ϕ) tilt systems is present, while for higher bismuth content $x \geqslant 0.3$ the orthorhombic tilt system is preferred.

It can be seen that the more relaxed polymorph is the main phase for each composition. This behavior can be explained by considering the structural distortions induced by the increase of $\langle r_B \rangle$. Thus, for $0.79 \leqslant \langle r_B \rangle \leqslant 0.81$ Å, the orthorhombic symmetry becomes pseudotetragonal with a maximum at $\langle r_B \rangle \approx 0.805$ Å ($x \approx 0.25$), where the tilt ($\phi^{-}_{O(2)} \backsimeq 8.33^\circ$) and the distortion of the octahedra ($\Delta_d \backsimeq 0.14 \times 10^{-3}\%$) give rise to a highly strained ($\delta \backsimeq 0.50\%$) orthorhombic lattice (Tables I and II). For $0.2 \leqslant x \leqslant 0.25$, the tetragonal phase is the relaxed polymorph since it exhibits lower octahedral distortion and tilting. However, for $x \geqslant 0.3$, the orthorhombic polymorph is favored because the tetragonal phase in this regime is highly strained due to the flattening of the octahedra ($d_c = 2.1402(10)$ Å, $d_{ab} = 2.164(8)$ Å $\rightarrow \Delta_d \backsimeq 2.71 \times 10^{-3}\%$) and the high tilting ($\phi^{-}_{O(2)} \backsimeq 8.33^\circ$). Also, the Pb[Bi]–O–Pb[Bi] bond angle (Θ) approaches 180° for the orthorhombic polymorph, while the structure becomes more distorted ($\ll 180^\circ$) for the tetragonal polymorph (Table II). Further, it is especially important to note that the minimum in the octahedral tilting angles for both the tetragonal and orthorhombic polymorphs is centered at the compositions where each phase displays its largest relative fraction. Also, these critical points in the octahedral tilting coincide with the compositions for the reported highest T_C ($x \approx 0.25$) and the M-S transition boundary ($x \approx 0.3$), as can be seen in Fig. 5. This fact suggests that the tetragonal polymorph is associated with the superconductivity, whereas the orthorhombic polymorph is related to the M-S transition for the BPBO system. That is, in the local picture, the mobility of the carrier pairs by dynamic exchange through the octahedra may be favored by the tetragonal symmetry, while a progressive localization of the carriers takes place on decreasing symmetry from the orthorhombic to the monoclinic phases with increasing bismuth content.

The temperature dependencies of the AC susceptibility χ' (real component) at frequency $f \backsimeq 10$ kHz and field $H_{ac} \backsimeq 5$ Oe are shown in Fig. 6(a). As noted in the introduction, the BPBO system for $0 < x \leqslant 0.30$ shows superconductivity. For $0.15 \leqslant x \leqslant 0.25$, the diamagnetic signal gradually increases with increasing x up to $x \approx 0.25$, for which the highest $T_C \backsimeq 12$ K is reached. However, in the composition range $0.25 < x \leqslant 0.35$, the tendency is reversed and for $x \approx 0.35$ (superconducting borderline and M-S transition boundary) the diamagnetic signal has vanished completely. Figure 6(b) shows the dc susceptibility χ data in the FC mode for $0.15 \leqslant x \leqslant 0.30$ as a function of the temperature, in the presence of a field $H_{dc} = 2$ Oe. The superconducting volume fraction estimated from FC data is always smaller than the true one due to flux pinning, trapping, and penetration length effects. However, the observed high-volume fraction in the FC data (>60% of the full diamagnetism $4\pi\chi_v = -1$) guarantees bulk superconductivity

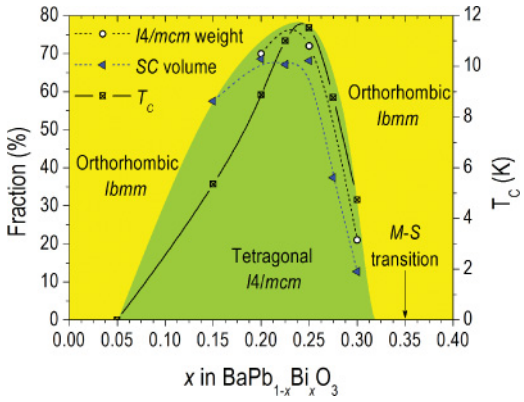

FIG. 7. (Color online) Composition evolution of the tetragonal polymorph weight fraction (dark green area), superconducting volume, and transition temperature (T_C) in BPBO for $0.05 \leqslant x \leqslant 0.30$. The arrow indicates the M-S transition. The dashed and solid lines are guides to the eye.

and can be roughly considered as the lower bound for the Meissner effect, that is, the superconducting volume fraction. Thus, for $0.15 \leqslant x \leqslant 0.25$, the estimated superconducting volume fraction increases with increasing x (from ~57 for $x \approx 0.15$ to ~69% for $x \approx 0.25$), whereas for $0.25 < x \leqslant 0.30$, decreases with increasing x (~13% for $x \approx 0.30$). It is important to notice that the estimated superconducting volume fraction remains almost constant (~68%) for $0.20 \leqslant x \leqslant 0.25$. The composition dependence of the superconducting volume fraction, the weight fraction of the tetragonal polymorph, and the superconducting T_C are depicted in Fig. 7. The trend in the superconducting volume fraction as a function of composition corresponds well with the evolution of the weight fraction of the tetragonal polymorph ($0.20 \leqslant x \leqslant 0.30$) estimated from the NPD data. This validates the suggestion that the tetragonal polymorph is directly connected with the superconductivity, and thus that tetragonal is the true symmetry for the superconducting phase.

These results can be considered in the context of what is seen for $Ba_{0.6}K_{0.4}BiO_3$ ($T_C \backsimeq 30$ K),[13,14] which exhibits superconductivity when the average symmetry is cubic. In BKBO, local probes of the structure have shown that locally the cubic symmetry is relaxed and there is local tilting of the octahedra.[43,44] It is experimentally observed that for both BPBO ($x \approx 0.25$ in $BaPb_{1-x}Bi_xO_3$, $\phi_{O(2)}^{-} \backsimeq 6.7^\circ$) and BKBO ($x \approx 0.40$ in $Ba_{1-x}K_xBiO_3$, $\phi \backsimeq 5^\circ$),[43,44] the T_C is highest when they adopt the highest possible average symmetry with the minimum octahedral tilting, even at their differing electron counts. Furthermore, if BKBO is compared with its lower average symmetry exact electronic analog $Sr_{0.4}K_{0.6}BiO_3$,[15] it is observed that the T_C drops dramatically from 30 to 13 K. These observations indicate that the structures, though differing in a subtle fashion, have a strong influence on the observed T_C, which may be due to either changes in orbital overlap and electronic energies or in the difference in phonon density of states in the different symmetry variants.

IV. CONCLUSIONS

The data presented in this work resolves the controversy related to the observed two-phase region in $BaPb_{1-x}Bi_xO_3$ for $0 < x \leqslant 0.30$. Our XRPD and NPD results at RT show that this region is actually a two-polymorph region in which the orthorhombic *Ibmm* and tetragonal $I4/mcm$ symmetries coexist for each composition. The coexistence of these polymorphs can be explained by considering the structural distortions induced in the orthorhombic *Ibmm* polymorph due to the increase of the effective size of the cation at the *B*-type site. Thus the distortions increase with increasing x for $0 < x \leqslant 0.25$, which suddenly provokes the onset of the relaxed tetragonal polymorph, by an instantaneous transition by 90° of the octahedral rotation axis from the $[110]_{pc}$ pseudocubic axis in *Ibmm* to the $[001]_{pc}$ pseudocubic axis in $I4/mcm$. However, on increasing the composition further, for $x \geqslant 0.3$ the tetragonal phase becomes more strained due to the internal distortion of the *B*-site octahedra, and the tendency is reversed. The onset and evolution of the tetragonal polymorph is accompanied by the onset and evolution of the superconductivity, as the estimated superconducting volume indicates, which suggests that this polymorph is directly correlated with the superconducting behavior. Therefore this work establishes the correlation between the average structure and the superconductivity and further that the competition between different structural polymorphs is strongest at exactly the optimal superconducting composition. This suggests that the structural instability that results in the change in rotation axes on going from the orthorhombic to the tetragonal polymorph may be involved in the superconducting mechanism, for example, through an enhanced susceptibility of these lattice modes in this composition region. Experimental studies of the optimal superconducting compositions in BPBO, even those employing local probes such as EXAFS and PDF (pair distribution function) analysis, should, however, be taken with strong caution; optimal superconducting samples will always be mixtures of superconducting and nonsuperconducting polymorphs unless thermodynamic equilibrium has been circumvented in the fabrication of the samples.

ACKNOWLEDGMENTS

The authors would like to thank M. Bremholm, S. Dutton, and J. M. Allred for helpful discussions. The work at Princeton University was supported by the AFOSR MURI on superconductivity.

[1] Y. Khan, K. Nahm, M. Rosenberg, and H. Willner, Phys. Status Solidi A, **39**, 79 (1977).
[2] A. W. Sleight, J. L. Gillson, and P. E. Bierstadt, Solid State Commun. **17**, 27 (1975).
[3] T. D. Thanh, A. Koma, and S. Tanaka, Appl. Phys. **22**, 205 (1980).
[4] T. Tani, T. Itoh, and S. Tanaka, *Proceedings of the 15th International Conference on the Physics of Semiconductors* [J. Phys. Soc. Jpn. **49**, 309 (1980)].
[5] B. Batlogg, Physica B **126**, 275 (1984).
[6] T. M. Rice and L. Sneddon, Phys. Rev. Lett. **47**, 689 (1981).

[7]S. Uchida, K. Kitazawa, and S. Tanaka, Phase Transitions **8**, 95 (1987).
[8]W. T. Fu, Physica C: Superconductivity **250**, 67 (1995).
[9]A. P. Menushenkov and K. V. Klementev, J. Phys. Condens. Matter **12**, 3767 (2000).
[10]C. Franchini, G. Kresse, and R. Podloucky, Phys. Rev. Lett. **102**, 256402 (2009).
[11]A. W. Sleight, Prog. Solid State Chem. **37**, 251 (2009).
[12]L. F. Mattheiss and D. R. Hamann, Phys. Rev. B **26**, 2686 (1982).
[13]L. F. Mattheiss, E. M. Gyorgy, and D. W. Johnson Jr., Phys. Rev. B **37**, 3745 (1988).
[14]R. J. Cava, B. Batlogg, J. J. Krajewski, R. Farrow, L. W. Rupp Jr., A. E. White, K. Short, W. F. Peck, and T. Kometani, Nature **332**, 814 (1988).
[15]S. M. Kazakov, C. Chaillout, P. Bordet, J. J. Capponi, M. Nunez-Regueiro, A. Rysak, J. L. Tholence, P. G. Radaelli, S. N. Putilin, and E. V. Antipov, Nature **390**, 148 (1997).
[16]D. E. Cox and A. W. Sleight, in *Proceedings of the Conference on Neutron Scattering, Gatlinburg, Tennessee*, edited by R. M. Moon (National Technical Information Service, Springfield, VA, 1976).
[17]A. W. Sleight and D. E. Cox, Solid State Commun. **58**, 347 (1986).
[18]M. Oda, Y. Hadika, A. Katsui, and T. Murakami, Solid State Commun. **55**, 423 (1985).
[19]M. Oda, Y. Hadika, A. Katsui, and T. Murakami, Solid State Commun. **60**, 897 (1986).
[20]H. Asano, M. Oda, Y. Endoh, Y. Hidaka, F. Izumi, T. Ishigaki, K. Karahashi, T. Murakami, and N. Watanabe, Jpn. J. Appl. Phys. **27**, 1638 (1988).
[21]J. Ihringer, J. K. Maichle, W. Prandl, A. W. Hewat, and T. Wroblewski, Z. Phys. B **82**, 171 (1991).
[22]H. Ritter, J. Ihringer, J. K. Maichle, W. Prandl, A. Hoser, and A. W. Hewat, Z. Phys. B **75**, 297 (1989).
[23]D. T. Marx, P. G. Radaelli, J. D. Jorgensen, R. L. Hitterman, D. G. Hinks, S. Pei, and B. Dabrowski, Phys. Rev. B **46**, 1144 (1992).
[24]V. R. R. Medicherla, T. Shripathi, and N. P. Lalla, J. Phys.: Condens. Matter **20**, 035219 (2008).
[25]S. M. Moussa, B. J. Kennedy, and T. Vogt, Solid State Commun. **119**, 549 (2001).
[26]W. T. Fu, D. Visser, and D. J. W. IJdo, Solid State Commun. **134**, 647 (2005).
[27]O. Moretzki, T. Doering, M. Steins, M. Wendschuh-Josties, and K. Bente, Z. Kristallogr. – New Cryst. Struct. **215**, 465 (2000).
[28]F. Abbattista, M. Vallino, A. Delmastro, D. Mazza, and S. Ronchetti, J. Solid State Chem. **117**, 55 (1995).
[29]J. Rodríguez-Carvajal and T. Roisnel, FULLPROF, WWINPLOTR, and accompanying programs, 2008; http://www.ill.eu/sites/fullprof/index.html (accessed January 2011).
[30]A. M. Glazer, Acta Cryst. B **28**, 3384 (1972). Glazer's notation: A measure of the lattice distortion from the ideal cubic perovskite structure is the degree of octahedral tilting. This notation adopts a pseudocubic multiple cell ($2a_{pc} \times 2b_{pc} \times 2c_{pc}$) to universally classify the tilting of BX_6 octahedra in each perovskite. The letters a, b, or c denote the magnitude of the rotation about each axis of the three Cartesian axes, and the superscripts $+$, $-$, and 0 indicate whether the rotations in adjacent layers are in the same (in-phase) or opposite (out-of-phase) direction, or if there is no rotation at all.
[31]B. C. Chakoumakos, S. E. Nagler, S. T. Misture, and H. M. Christen, Physica B **241-243**, 358 (1997).
[32]B. J. Kennedy and B. A. Hunter, Phys. Rev. B **58**, 653 (1998).
[33]B. J. Kennedy, B. A. Hunter, and J. R. Hester, Phys. Rev. B **65**, 224103 (2002).
[34]W. T. Fu, D. Visser, K. S. Knight, and D. J. W. IJdo, J. Solid State Chem. **177**, 1667 (2004).
[35]M. Glerupa, K. S. Knight, and F. W. Poulsen, Mater. Res. Bull. **40**, 507 (2005).
[36]B. J. Kennedy, L. Li, R. F. Garrett, Y. Kubota, and K. Kato, Solid State Commun. **122**, 355 (2002).
[37]S. K. Mishra, R. Ranjan, D. Pandey, P. Ranson, R. Ouillon, J. P. Pinan-Lucarre, and P. Pruzan, J. Phys. Condens. Matter **18**, 1899 (2006).
[38]B. J. Kennedy, C. J. Howard, G. J. Thorogood, and J. R. Hester, J. Solid State Chem. **161**, 106 (2001).
[39]E. H. Mountstevens, J. P. Attfield, and S. A. T. Redfern, J. Phys. Condens. Matter **15**, 8315 (2003).
[40]R. D. Shannon, Acta Cryst. A **32**, 751 (1976).
[41]K. S. Aleksandrov, Ferroelectrics **14**, 801 (1976). Aleksandrov's notation: Aleksandrov uses an approach similar to Glazer in describing perovskite distortions, using ψ and ϕ to represent the in-phase and out-of-phase rotations, respectively, and the subscript numbers 1, 2, or 3 to denote the magnitude of the rotation, e.g., $a^0a^0c^-$ is written as 00ϕ, and $a^+b^+c^-$ is written as $\psi_1\psi_2\phi$.
[42]B. J. Kennedy, C. J. Howard, and B. C. Chakoumakos, J. Phys. Condens. Matter **11**, 1479 (1999).
[43]Y. Yacoby, S. M. Heald, and E. A. Stern, Solid State Commun. **101**, 801 (1997).
[44]N. V. Anshukova, A. I. Golovashkin, V. S. Gorelik, L. I. Ivanova, and A. P. Rusakov, J. Mol. Struct. **219**, 147 (1990).